

# Gamma Ray and Hadron generated Čerenkov Photon Spectra at Various Observation Altitudes

M. A. Rahman, P. N. Bhat, B. S. Acharya, V. R. Chitnis,  
P. Majumdar and P. R. Vishwanath  
*Tata Institute of Fundamental Research,  
Homi Bhabha Road, Colaba, Mumbai 400 005, India.*

August 18, 2019

## Abstract

We study the propagation of Čerenkov photons generated by Very High Energy  $\gamma$ -rays and hadrons in the atmosphere. The photon production height distributions are estimated from semi-empirical methods and compared with those derived by standard simulation techniques. Incident spectra at various observation altitudes are then derived after applying wavelength dependent corrections due to photon attenuation in the atmosphere during the propagation of photons from the height of production to the height of observation. These are generated both for  $\gamma$ - and hadron primaries of various energies. The derived production height distributions agree very well with those generated by the simulation package ‘CORSIKA’ at all energies and for both  $\gamma$ -ray and proton primaries. The incident photon spectra are found to be both altitude dependent and primary energy dependent. The peak of the incident spectrum shifts towards the shorter wavelength with increasing altitude of observation for a given primary. Also the peak of the photon spectrum shifts towards the shorter wavelength with increasing energy of the primary at given altitude. The fraction of the UV component in the incident Čerenkov spectrum is

estimated both for  $\gamma$ -ray and hadronic primaries at various observation altitudes and energies. Hadron generated Čerenkov spectra are marginally richer in UV light and the difference increases slightly at higher altitudes. The fraction of the UV to the visible light in the Čerenkov spectrum could be a useful parameter to separate  $\gamma$ -rays from cosmic ray background only if one can measure this fraction very accurately.

## 1 Introduction

In the highest energy end of the electromagnetic spectrum, the energy range between 50 keV and 30 GeV has been successfully covered by satellite based missions[1]. At higher the energies steeply falling spectrum makes it impossible to observe the  $\gamma$ -ray sky by satellite based detectors. The ground based atmospheric Čerenkov technique has proved to be the most sensitive technique in exploring the celestial  $\gamma$ -rays in the energy range 300 GeV - 10 TeV. The basic detection technique in this case is to deploy one or several parabolic mirrors at the observation level fitted with fast photo tubes at the focus. Very high energy celestial  $\gamma$ -rays initiate an electromagnetic cascade in the atmosphere as they enter the atmosphere. The electrons and positrons in the cascade, being relativistic, emit Čerenkov light as they propagate down the atmosphere resulting in a faint ( $\sim 10^{-4}$  times the brightness of the star light background) flash of light lasting a few nanoseconds. This fast Čerenkov flash is detected electronically by coincidence technique. However the main drawback of the technique is the presence of much more abundant cosmic ray background which severely limit the sensitivity of this technique. Various ingenious techniques are employed to distinguish between the Čerenkov light produced by cosmic  $\gamma$ -rays from that by the cosmic rays. Among these, the imaging technique, wavefront sampling technique, angular and spectral separation techniques are currently employed by different experiments [2, 4, 3, 5].

In spite of the necessity of carrying out these observations during clear, moon-less nights which scales to only about 10-15% duty cycle, the technique has been successful mainly due to two reasons. Firstly, a large collection area which is  $\sim 10^4 - 10^5$  times larger than the satellite detectors provides a high event rate. Secondly, with high angular resolution and some recently developed  $\gamma$ - hadron separation techniques [3, 6] provide high sensitivity to the method. Large ground based telescopes based on this technique are now being built to cover the intermediate energy range of 30 - 300 GeV [39, 35, 37, 40].

In the absence of standard mono-energetic beams of cosmic rays or  $\gamma$ -rays, one has to depend on the simulation techniques to understand and optimize the detector response to these radiations. For this purpose we have carried out detailed simulations with VHE  $\gamma$ -rays and cosmic rays of various pri-

mary energies initiating extensive air showers in the atmosphere. In order to ensure the reliability of the conclusions drawn from these studies it is imperative to verify the correctness of the basic results derived from these simulations. There are a few simulation packages painstakingly developed by high energy physicists and we chose one of them called CORSIKA [8] developed by the KASCADE collaboration.

CORSIKA (version 562), [8, 7] has been used here to simulate Čerenkov light emission in the earth's atmosphere by the secondaries of the extensive air showers generated by cosmic ray primaries or  $\gamma$ -rays. This program simulates interactions of nuclei, hadrons, muons, electrons and photons as well as decays of unstable secondaries in the atmosphere. It uses EGS4 code [9] for the electromagnetic component of the air shower simulation and GHEISHA[10] for the simulation of hadronic interactions at TeV energies. The Čerenkov radiation produced within the specified bandwidth (300-550  $nm$ ) by the charged secondaries is propagated to the ground. The US standard atmosphere parameterized by Linsley [12] has been used. The position, angle, time (with respect to the first interaction) and production height of each Čerenkov photon hitting the detector at the observation level are recorded.

We have mainly used Pachmarhi (longitude:  $78^{\circ} 26'$  E, latitude:  $22^{\circ} 28'N$  and altitude:  $1075 m$ ) as the observer's location where an array of 25 Čerenkov detectors each of area  $4.35 m^2$  is deployed in the form of a rectangular array. We have assumed 17 detectors in the E-W direction with a separation of  $25 m$  and 21 detectors in the N-S direction with a separation of  $20 m$ . This configuration, similar to the Pachmarhi Array of Čerenkov Telescopes (PACT) [13] but much larger, is chosen so that one can study the core distance dependence of various observable parameters. Simulations were also carried out at sea level and a location at an altitude of  $2 km$  above mean sea level. Mono-energetic primaries consisting of  $\gamma$ - rays and protons incident vertically on the top of the atmosphere with their cores at the centre of the array have been simulated in the present study.

The longitudinal shower development profiles of Čerenkov photons in the atmosphere have been generated using CORSIKA for  $\gamma$ -ray and proton primaries of various energies. Tracks of charged particles are followed through in steps  $20 g cm^{-2}$  [14, 31].

In the present work the Čerenkov photon growth curves have been obtained from the simulations for proton and  $\gamma$ -ray primaries of various energies and for the three observation levels mentioned above. These have been compared with those derived from independent empirical relations. The Čerenkov photon spectra as seen at the observation levels are then derived for various primary energies of  $\gamma$ -rays and protons after taking into account of the wavelength dependent attenuation in the atmosphere. Then we estimate the relative fraction of UV photons in these spectra as a function of

primary energy and observation level.

## 2 Calculation of longitudinal profiles

### 2.1 $\gamma$ -ray primaries

For showers initiated by photons of energy  $E_\gamma$  the longitudinal shower development curve is derived from the equation for cascade curve under approximation A. The average number of electrons of all energies  $N(E_\gamma, x)$  as a function of atmospheric depth  $x$ , is given approximately, in the region where the number of particles is large, by [32]:

$$N(E_\gamma, x) = \frac{0.31}{\sqrt{\ln\left(\frac{E_\gamma}{E_t}\right)}} \exp(t(1 - 1.5 \ln s))$$

where  $t$  is the depth  $x$  measured in units of radiation length in the atmosphere ( $37.2 \text{ g cm}^{-2}$ ) and  $E_t$  is the the electron critical energy at the depth  $t$ . This is the energy below which the electron multiplication stops. It is approximately the energy at which radiation losses and collisional losses are equal and has a value 84.2 MeV in air. The shower age parameter,  $s$ , which is a measure of the stage of the longitudinal shower development, is given by:

$$s = \frac{3t}{(t + 2 \ln \frac{E_\gamma}{E_t})}$$

$s = 1$  at shower maximum while  $s < 1$  above the shower maximum and  $s > 1$  below. The relation between the atmospheric height  $h$ , (as measured from sea level in  $m$ ) and the depth,  $x$  ( $\text{g cm}^{-2}$  as measured from the top of atmosphere) is taken from Rao[33]:

$$h = (6740 + 2.5x) \ln\left(\frac{1030}{x}\right) \quad m$$

where the scale height is dependent on the atmospheric depth. The refractive index  $n$  at a given height  $h$  is assumed to be:

$$n = 1 + n_0$$

where  $n_0$  is given by:

$$n_0 = 2.9 \times 10^{-4} e^{-\frac{h}{7100}}$$

For calculating the electron growth curve the atmosphere is divided into slabs of thickness 333  $m$ , after the height of first interaction of the primary. The electron threshold energy for the production of Čerenkov radiation at a depth  $t$  is given by

$$E_{th} = \left( \frac{1}{\sqrt{1 - (1 + n_0)^{-2}}} - 1 \right) m_e$$

where  $m_e$  is the electron rest mass (0.51 MeV). The fraction of electrons with energy above the Čerenkov threshold is given by [16]:

$$f_{\check{C}} = \left( \frac{0.89E_0 - 1.2}{E_0 + E_{th}} \right)^s (1 + 0.0001sE_{th})^{-2}$$

where  $E_0 = 26 \text{ MeV}$  when  $s \leq 0.4$

$$= 44 - 17(s - 1.46)^2 \text{ MeV for } s > 0.4$$

The number of electrons above the Čerenkov threshold is then computed in each of the slabs. For each straight section of the electron path, the number of Čerenkov photons produced per unit path-length is given by,

$$\frac{dN}{dl} = 6.28\alpha \left( \frac{1}{\lambda_1} - \frac{1}{\lambda_2} \right) \left( 1 - \frac{1}{\beta^2 n^2} \right)$$

in the wavelength band bounded by  $\lambda_1$  and  $\lambda_2$  and  $\beta$  is the electron velocity and  $\alpha$  is the fine structure constant. Assuming all the electrons in the cascade to be close to the shower axis and they travel with the velocity close to that of light in vacuum, the number of Čerenkov photons produced in a path-length  $dl$  ( $= 333 \text{ m}$  in the present case) and in the wavelength range 300-550  $\text{nm}$  at a depth  $x \text{ g cm}^{-2}$  is then given by,

$$N_{ph} = 0.402N \left( \frac{x}{1030} \right) dl$$

## 2.2 Proton primaries

Because of the differences in the kinematics of shower development in the case of hadronic primaries the longitudinal development profiles too are different as compared to that of  $\gamma$ -ray primaries. Using the scaling model for nuclear interactions, Gaisser & Hillas [17] find that the average number of particles,  $N(E_p, x)$  at an atmospheric depth of  $x \text{ g cm}^{-2}$ , measured from the first point of interaction, in a shower initiated by a proton of energy  $E_p$  (GeV) can be adequately represented by the empirical relationship [20, 11]

$$N(E_p, x) = S_0 \frac{E_p}{\epsilon} e^{t_m} \left( \frac{t}{t_m} \right)^{t_m} e^{-t}$$

where

$$t_m(E_p) = \frac{x_0}{\lambda} \ln \left( \frac{E_p}{\epsilon} \right) - 1$$

where  $S_0=0.045$ ,  $\epsilon=0.074$ ,  $x_0 = 37.2 \text{ g cm}^{-2}$ ,  $t = \frac{x}{\lambda}$  and  $\lambda$  =proton interaction mean free path in air ( $70 \text{ g cm}^{-2}$ ). We chose the electron energy spectrum

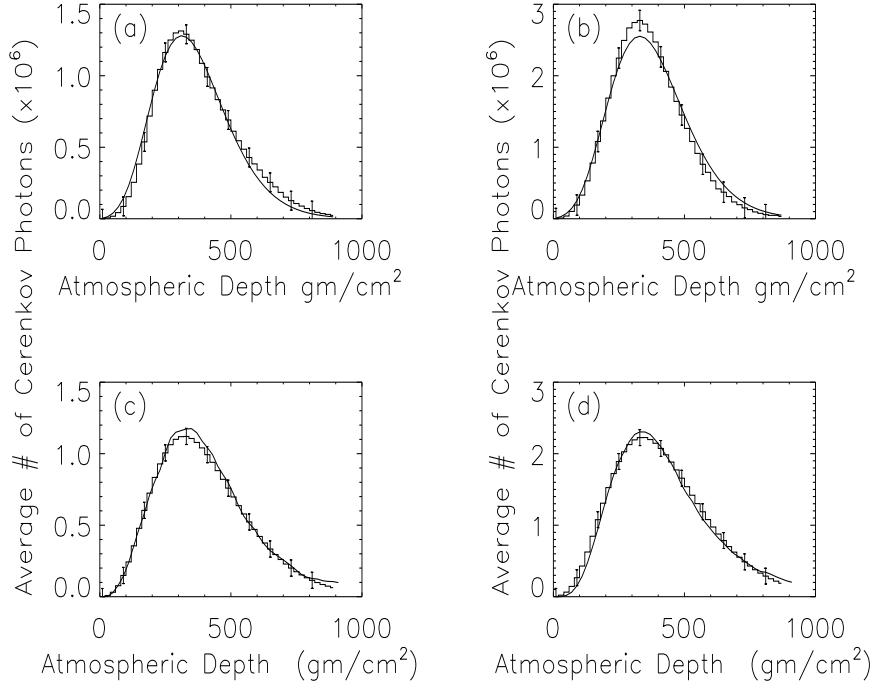


Figure 1: Čerenkov photon growth curves in the atmosphere for  $\gamma$ - ray of (a) 500 GeV & (b) 1 TeV and protons of (c) 1 TeV & (d) 2 TeV primaries. The histograms indicates the simulation results from CORSIKA while the smooth curves indicates the results from analytical calculations. The agreement between the two curves is good.

given by Zatsepin and Chudakov which is independent of the stage of cascade development [20, 21].

$$F(E, x) dE = 0.75 N(x) \frac{d\delta}{1 + \delta}$$

where  $F(E, x)$  and  $N(x)$  are the number of electrons of energy  $E$  and all energies respectively at a depth  $x$ ,  $\delta = 2.3E/\kappa$  and  $\kappa = 72$  MeV with  $E$  in MeV. Even though this approximates well at shower maximum in the energy range 20-300 MeV, the minor departure at other depths affects only the shape of the lateral distribution of Čerenkov photons and does not affect the present estimates significantly. The integral electron energy spectrum is then derived:

$$F(E, x) = 0.75 N(x) \ln \left( 1 + \frac{2.3}{\kappa} E \right)$$

Substituting  $E_{th}$  for  $E$ , the number of electrons above the Čerenkov threshold at a particular depth are calculated using the above equation.

Table 1: Quantitative comparison of the simulated and calculated Čerenkov photon growth curves in the atmosphere for  $\gamma$ -ray and proton primaries at two primary energies.

Results from	Type of primary	Energy of primary (GeV)	Total # of Čerenkov photons ( $\times 10^7$ )
Simulations	$\gamma$ - rays	500	2.25
	Protons	1000	2.35
	$\gamma$ - rays	1000	4.55
	Protons	2000	4.81
Calculations	$\gamma$ - rays	500	2.22
	protons	1000	2.35
	$\gamma$ - rays	1000	4.56
	protons	2000	4.72

The longitudinal Čerenkov photon profiles are then derived for  $\gamma$ -rays of primary energy 50, 100, 250, 500 and 1000 GeV and protons of energy 100, 200, 500, 1000 and 2000 GeV. The growth curves are simulated using CORSIKA for two primary energies for  $\gamma$ -rays (500 GeV & 1000 GeV) and protons (1000 & 2000 GeV). Figure 1 shows a comparison of the simulated longitudinal profiles for  $\gamma$ - rays (a & c) as well as protons (b & d) with calculated profiles. The simulated profiles (histograms) are averaged over 30 showers for  $\gamma$ - rays and 50 showers for protons. The agreement between the simulated and calculated longitudinal shower development profiles in terms of Čerenkov photons is good for  $\gamma$ -ray as well as proton primaries of energies considered here. Table 1 summarizes the total number of Čerenkov photons in these showers. The total number of Čerenkov photons agree with that from simulations within 1 & 2% for  $\gamma$ -ray and proton primaries respectively.

The depth of shower maximum is expected to increase logarithmically with primary energy both for electromagnetic as well as hadronic showers as more cascade generations are required to degrade the secondary particle energies [20, 11]. Figure 2 shows a plot of the depth of shower maximum as a function of primary energy, both for  $\gamma$ -ray and proton primaries in order to illustrate this point as well as to confirm the correctness of the present calculations. The energy dependence of the depth of shower maximum is parameterized as follows:

$$x_{max} = 30.3 \ln E_{\gamma} + 118.8 \quad g \text{ cm}^{-2}$$

for  $\gamma$ -rays and,

$$x_{max} = 32.6 \ln E_p + 118.6 \quad g \text{ cm}^{-2}$$

for protons.

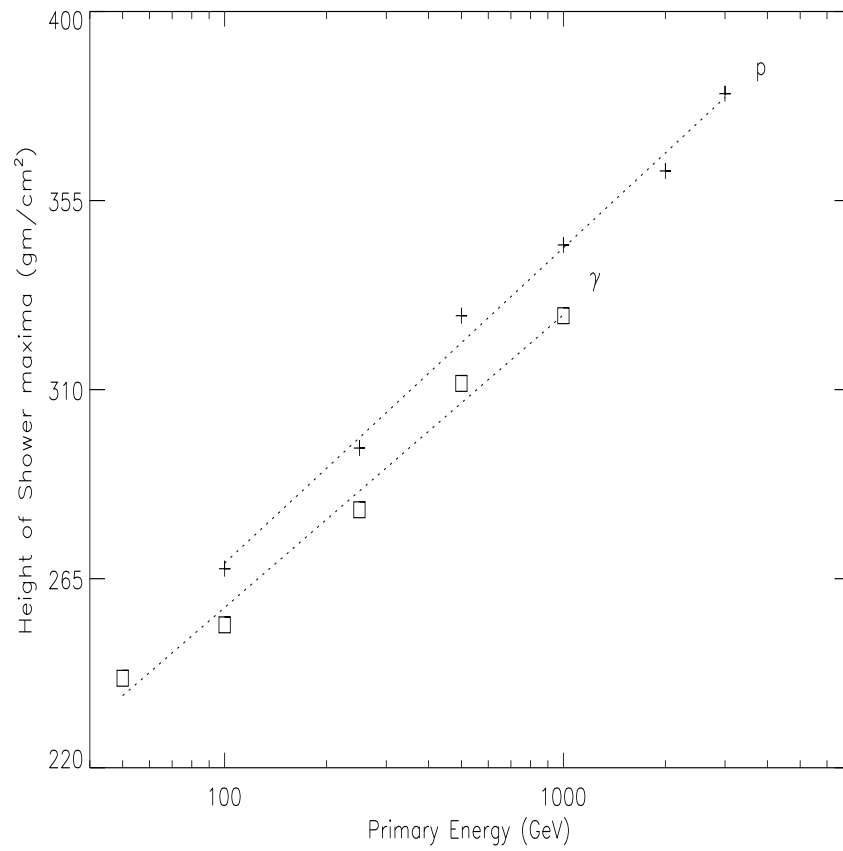


Figure 2: The variation of the depth of shower maximum with primary energy for  $\gamma$ -rays and protons.



### 3 Photon attenuation in the atmosphere

To study the attenuation of Čerenkov light in the atmosphere Elterman's atmospheric attenuation model [22] is used, which provides the attenuation coefficients for the Rayleigh and aerosol scattering as well as ozone absorption in an altitude dependent form for the wavelength range 270-1260 *nm* [22].

Atmospheric attenuation model computes optical parameters spectrally and with altitude as follows: (1) pure air attenuation parameters are determined by utilizing Rayleigh scattering cross sections with molecular number densities from standard atmosphere; (2) ozone absorption parameters are derived from coefficients applied to a representative atmospheric ozone distribution; (3) seven sets of aerosol measurements are compared and a profile of aerosol attenuation coefficients as a function of altitude is developed. Tabulation permits calculations for vertical path transmission at one kilometer intervals up to an altitude of 50 *km*, individually for each attenuating component or for overall atmospheric extinction (molecular + ozone + aerosol). Above 700 *nm* light of night sky (LONS) increases rapidly because of emission lines of OH and water bands in upper atmosphere while the intensity of Čerenkov light drops considerably( inversely proportional to the square of wavelength). At lower wavelengths (< 300 *nm*) light undergoes strong absorption by ozone molecules in the upper atmosphere.

The number of photons, integrated over the bandwidth of 300-550 *nm* (dictated by the photo-tube band-width) and transmitted through a slab (1 *km* thick) using the corresponding extinction coefficient is given by:

$$N = N_1 e^{-B}$$

where N is the number of photons transmitted through the slab with absorption coefficient B and  $N_1$  is the mean number of photons entering the slab. For each altitude, the photon transmission spectrum is convolved with the Čerenkov photon emission spectrum to get the transmitted photon spectrum. Showers pass through several such slabs with different transmission coefficients, resulting in a modified longitudinal development profile for the Čerenkov photons that reach the observation level. The ratio of the total number of photons within the band-width in a shower received at a particular observation level to the total photons produced is defined as the transmission coefficient. The average transmission coefficients ( $T_c$ ) are listed in tables 2 and 3 for  $\gamma$ -ray and proton primaries respectively for Pachmarhi altitude.  $T_c$  can be expressed as a power law in primary energy, E as

$$T_c = aE^b \tag{1}$$

The values of  $a$  and  $b$  are listed in table 4 both for  $\gamma$ -ray and proton primaries at three different observation levels. The variation in the average transmission coefficients for Čerenkov photons in the atmosphere is shown

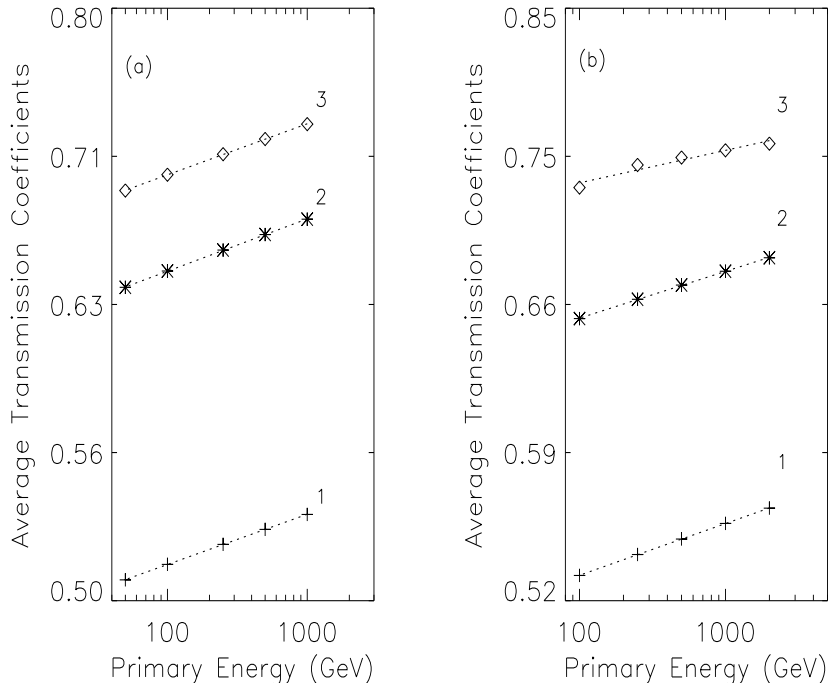


Figure 3: Average transmission coefficient for Čerenkov photons in the atmosphere for primary (a)  $\gamma$ -rays and (b) protons of various energies. The straight lines show the fits. The three plots in each panel correspond to three observation levels (1) sea level, (2) Pachmarhi (1 km a.s.l.) and (3) 2 km (a.s.l.) altitude.

in figure 3 for (a)  $\gamma$ -ray and (b) protons as a function of primary energy at three different observation levels, illustrating the power law behavior.

The increase in  $T_c$  with primary energy implies that higher energy primaries penetrate deeper in the atmosphere and hence pass through lesser air mass. The proton primaries reach the shower maximum lower down in the atmosphere compared to a  $\gamma$ -ray primary of the same energy since the interaction mean free path in air for the former is nearly twice the radiation length. As a result the protons have marginally larger ( $\sim 1.2\%$  at 100 GeV to  $\sim 0.6\%$  at 1 TeV) average transmission coefficient compared to a  $\gamma$ -ray primary of the same energy.

The attenuation of optical photons due to Rayleigh and aerosol scattering is more significant at lower altitudes. As a result the Čerenkov photon transmission is expected to depend on the observation level as also seen in figure 3. The average photon transmission coefficient increases almost linearly with decreasing atmospheric depth and the rate is  $\sim 0.1\%$  for every  $100 g cm^{-2}$  of air.

Figure 4 shows the longitudinal development profiles of Čerenkov photons

Table 2: Shower size and average transmission coefficients corresponding to Pachmarhi altitude for primary  $\gamma$ -rays of various energies (band-width: 300-550  $nm$ ).

Primary energy (GeV)	# of $\check{C}$ Photons		Average Transmission coefficient	Depth of shower max. ( $g\ cm^{-2}$ )
	produced	transmitted		
50	$2.02 \times 10^6$	$1.29 \times 10^6$	0.641	241.3
100	$4.16 \times 10^6$	$2.70 \times 10^6$	0.649	254.0
250	$1.08 \times 10^7$	$7.14 \times 10^6$	0.660	281.4
500	$2.22 \times 10^7$	$1.48 \times 10^7$	0.669	311.5
1000	$4.54 \times 10^7$	$3.07 \times 10^7$	0.677	327.6

Table 3: Shower size and average transmission coefficients corresponding to Pachmarhi altitude for primary protons of various energies (band-width: 300-550  $nm$ ).

Primary energy (GeV)	# of $\check{C}$ photons		Average transmission coefficient	Depth of shower max. ( $g\ cm^{-2}$ )
	produced	transmitted		
100	$2.17 \times 10^6$	$1.42 \times 10^6$	0.657	267.4
250	$5.56 \times 10^6$	$3.70 \times 10^6$	0.665	296.1
500	$1.15 \times 10^7$	$7.74 \times 10^6$	0.673	327.6
1000	$2.37 \times 10^7$	$1.61 \times 10^7$	0.681	344.5
2000	$4.86 \times 10^7$	$3.34 \times 10^7$	0.688	362.1

Table 4: Fitted coefficients  $a$  and  $b$  in equation 1 for  $\gamma$ -ray and proton primaries at three different observation levels.

Observation level $km$ a.s.l.	Fitted coefficients	$\gamma$ -rays	Protons
0 (Sea level)	$a$	0.475	0.487
	$b$	0.018	0.019
1	$a$	0.598	0.608
	$b$	0.018	0.017
2	$a$	0.646	0.697
	$b$	0.018	0.012

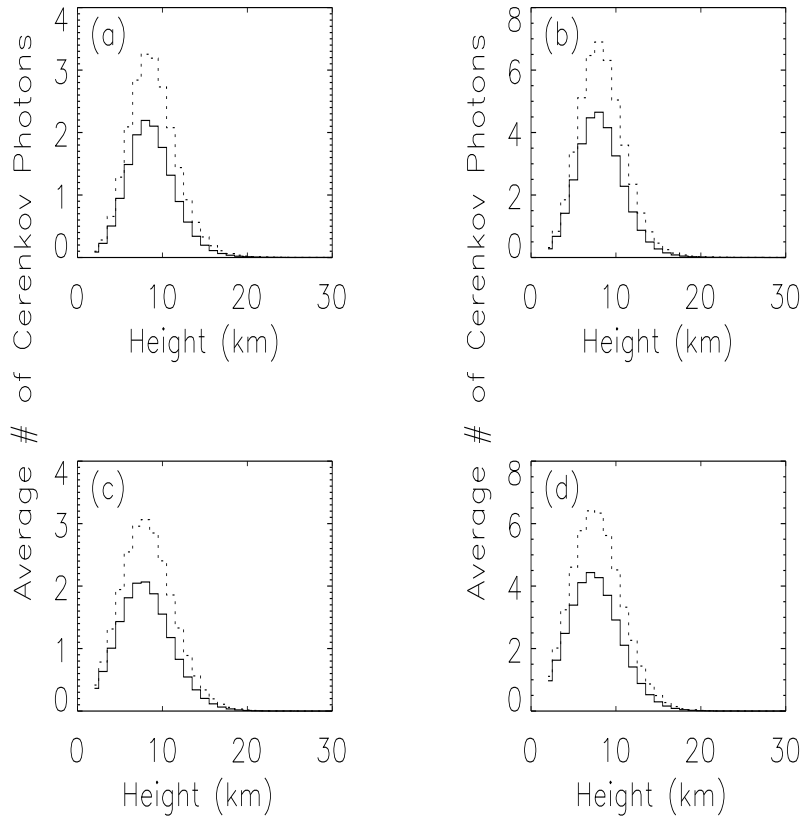


Figure 4: A comparison of the longitudinal development profiles of Čerenkov photons at Pachmarhi level with and without atmospheric attenuation correction. *a* & *b* are for  $\gamma$ -ray primaries of energy 50 GeV and 1 TeV respectively while *c* & *d* are for proton primaries of energy 100 GeV and 2 TeV respectively (band-width: 300-550 nm).

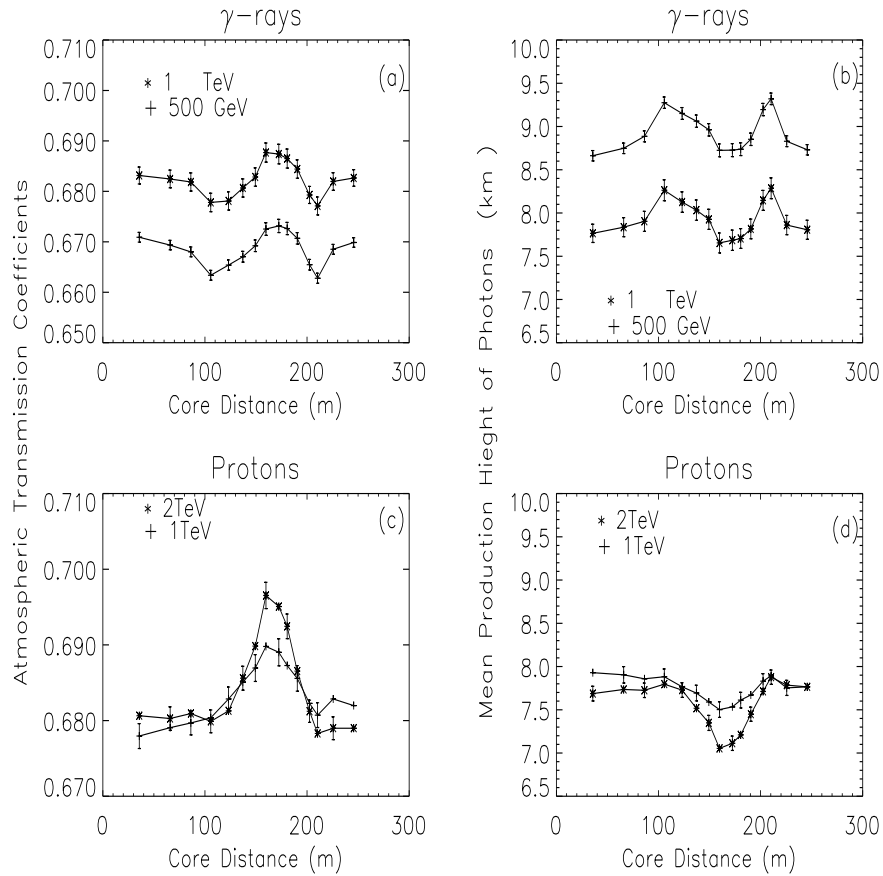


Figure 5: Radial dependence of the Čerenkov photon transmission coefficients in the atmosphere for (a)  $\gamma$ -ray and (c) proton primaries of two different primary energies as shown. Also shown are the radial dependence of average production heights for each of the primaries (b & d respectively) and their energies mentioned above. Simulation results are averages over 43 & 17  $\gamma$ -ray showers of primary energy 500 GeV and 1 TeV respectively while 47 showers are used for 1 & 2 TeV proton primaries.

at production in the atmosphere and that for the photons detected at the observation level (*i.e.* “without” and “with” atmospheric attenuation correction) for the same wavelength band. The differences in the two profiles is due to the wavelength dependent absorption of Čerenkov photons in the atmosphere. From the plots it is clear that the shape of the longitudinal profile remains largely unchanged (except for the total number of photons). The range of atmospheric heights from which the detected photons originate also remains unchanged as well, irrespective of the primary energy or species. Thus the height of shower maximum remains unchanged due to atmospheric attenuation.

The average path-length of Čerenkov photons reaching different core dis-

tances differ resulting in different attenuation. Figure 5 shows such a radial variation of the transmission coefficient for Čerenkov photons generated by  $\gamma$ -rays and protons of two different energies. Also shown are the radial variation of mean production heights. It can be seen that the radial variation of transmission coefficients is rather small but varies inversely as the mean production height.

## 4 Čerenkov photon spectrum

The Čerenkov photon spectrum at the observation level is an important input for the design of an atmospheric Čerenkov experiment. The fraction of the photon spectrum bracketed by the photo-multiplier bandwidth has an important bearing on the sensitivity of a TeV  $\gamma$ -ray telescope. Hence we computed the photon spectrum at different observation levels for  $\gamma$ -ray and proton primaries of various energies. The bandwidth considered in our calculation is 270-550 *nm*. Figure 6 shows photon spectra, corresponding to Pachmarhi level, generated by (a) 50 GeV  $\gamma$ -rays & 100 GeV protons (\* & diamond respectively) as well as (b) 1 TeV  $\gamma$ -rays & 2 TeV protons. It can be seen from the figure that the wavelength at peak intensity is a function of the primary energy in both the cases. It shifts from around 350 *nm* at 50 GeV to around 330 *nm* at 1 TeV. This is because the higher energy primaries reach the shower maximum lower down in the atmosphere compared to lower energy primaries. As a result, absorption of shorter wavelength photons which is primarily due to atmospheric Ozone is comparatively larger for lower energy primaries.

### 4.1 Fraction of UV component at various altitudes

The UV filters were used in atmospheric Čerenkov experiments [23] whose purpose was two-fold: firstly, it helps reduce night sky background while minimizing the loss of Čerenkov light in the blue and near UV range. This would provide better stability at higher photo-tube gains which in turn will improve the sensitivity of an atmospheric Čerenkov telescope. Secondly, it could serve to identify showers with a larger UV fraction in the Čerenkov light. Since the Čerenkov light generated by proton primaries traverse lesser air mass as compared to  $\gamma$ -ray primaries it is expected to have a larger UV content. This property could be exploited to discriminate against hadronic showers [24].

Hence the UV fraction in Čerenkov light at observation level is a useful signature. So we estimated this fraction for primaries of various energies. We divided the Čerenkov photon spectrum as seen at the observation level into two groups *viz.*, the UV range comprising wavelengths 270-300 *nm* and the visible range comprising the wavelength band 300-550 *nm*. The ratio of the

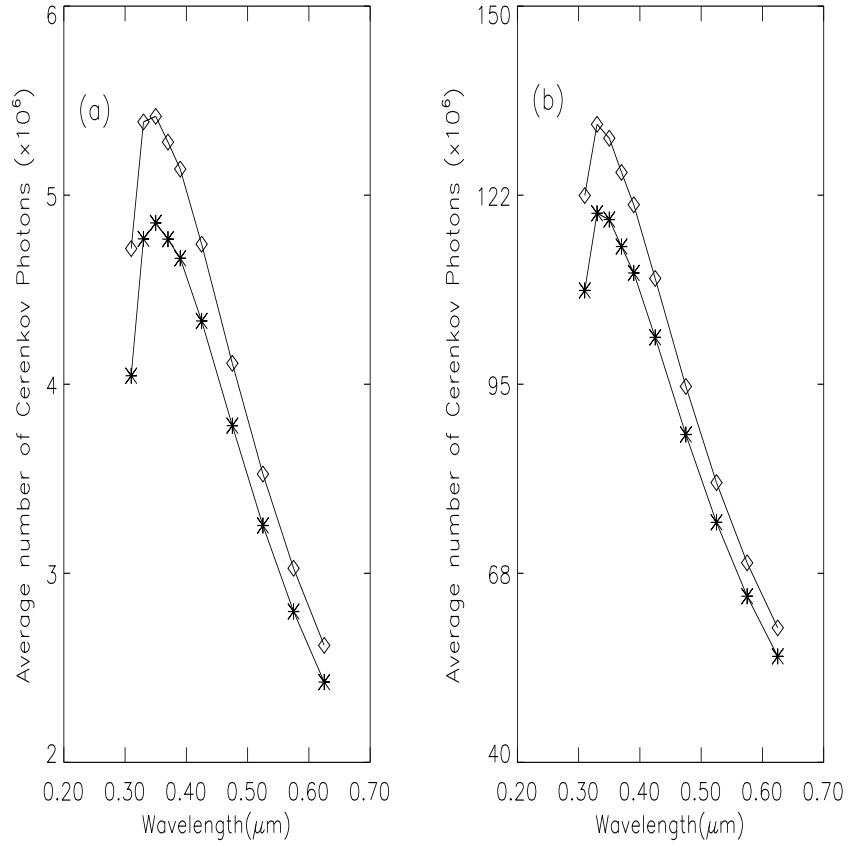


Figure 6: Typical Čerenkov photon spectra at Pachmarhi level. (a) shows the spectra from  $\gamma$ -ray primaries of energy 50 GeV and 100 GeV protons while (b) shows those for 1 TeV  $\gamma$ -ray & 2 TeV proton primaries. The symbols used are \* for  $\gamma$ -rays and diamond for protons.

Table 5: Ratio of UV (270-300 *nm*) to visible (300-550 *nm*) component in the Čerenkov light detected at three observation altitudes as a function of  $\gamma$ -ray and proton energies.

Primary energy (GeV) $E_\gamma/E_p$	Sea level		1 <i>km</i>		2 <i>km</i>	
	$R_\gamma$ (%)	$R_p$ (%)	$R_\gamma$ (%)	$R_p$ (%)	$R_\gamma$ (%)	$R_p$ (%)
50 / 100	8.23	9.57	8.27	9.67	8.29	9.77
100/200	8.26	9.59	8.29	9.69	8.33	9.80
250/500	8.29	9.60	8.32	9.71	8.37	9.85
500/1000	8.31	9.61	8.34	9.72	8.41	9.88
1000/2000	8.32	9.61	8.36	9.73	8.44	9.91

number of photons in the UV range to that in the visible range is defined as  $R_p$  for proton primaries and  $R_\gamma$  for  $\gamma$ -ray primaries. Table 5 summarizes the  $R_\gamma$  and  $R_p$  values for different primary energies as seen at three different observation altitudes.

Figure 7 shows a plot of  $R_p$  and  $R_\gamma$  as a function of primary energy for three different observation levels. Also shown in figure 7 are the relative excess of UV content in proton showers *vis-a-vis*  $\gamma$ -ray showers, as a function of primary energy at three different altitudes.

It can be readily seen from the figure that sensitivity to UV excess is better at higher altitudes as compared to sea level.

Figure 8 shows radial variation of the ratio of UV to visible photons for  $\gamma$ -ray and proton primaries at an altitude of 1 *km*. The relative UV fraction is marginally higher around the hump region since the photons in this region are contributed by higher energy electrons which have shortest path-length in air. The radial dependence of the UV fraction is more pronounced for proton primaries for reasons already mentioned before.

## 5 Discussion and Conclusions

In spite of the complexity of the interaction kinematics of high energy cosmic rays in the atmosphere, the average behavior as derived from detailed simulation studies agrees reasonably well with analytical calculations. This demonstrates that the simulation package does take into account almost all the interaction characteristics giving credence to the conclusions drawn from simulation studies. The position of shower maximum obtained by us agrees well with those of Miller & Westerhoff [28].

Armed with the above result we proceed to make analytical calculations for the production of Čerenkov light produced by both  $\gamma$ -rays and protons of various energies at three different observation altitudes. This is ideal to



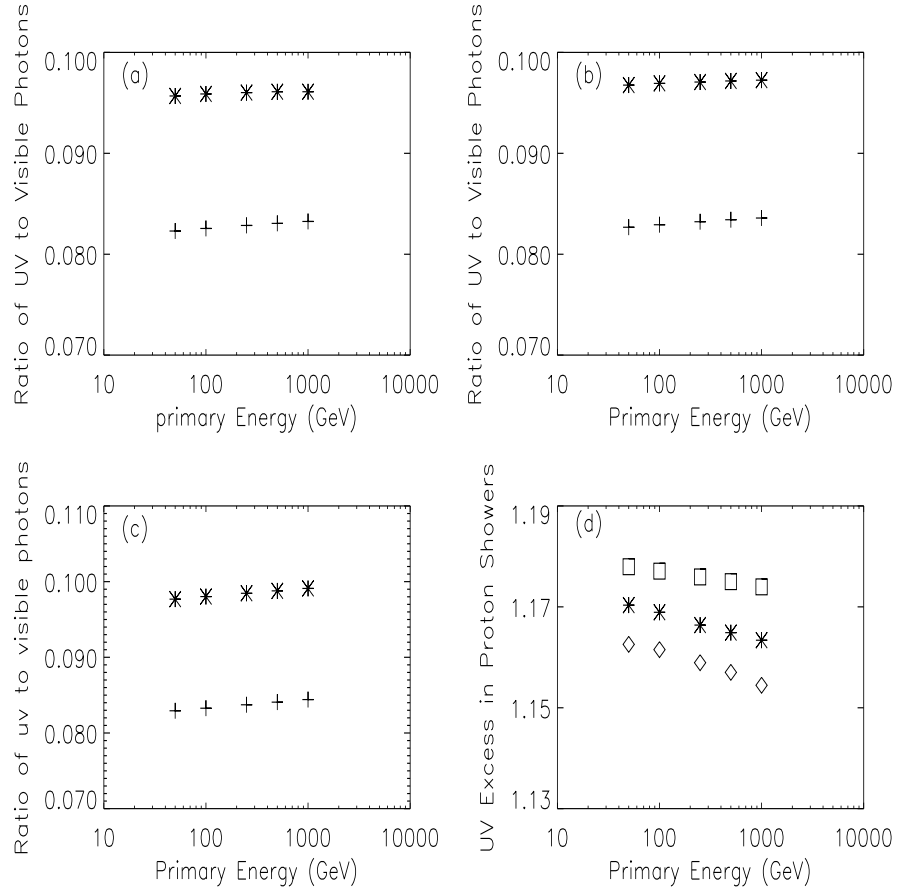


Figure 7: Variation of the ratio of UV to visible fraction in Čerenkov light generated by protons (\*) and  $\gamma$ -rays (+) as a function of primary energy, at three observation levels: (a) sea level (b) Pachmarhi and (c) 2 km a.s.l. (d) The relative excess in the UV content in hadronic primaries as a function of primary energy expected at three different observation levels, in the same order from bottom to top.

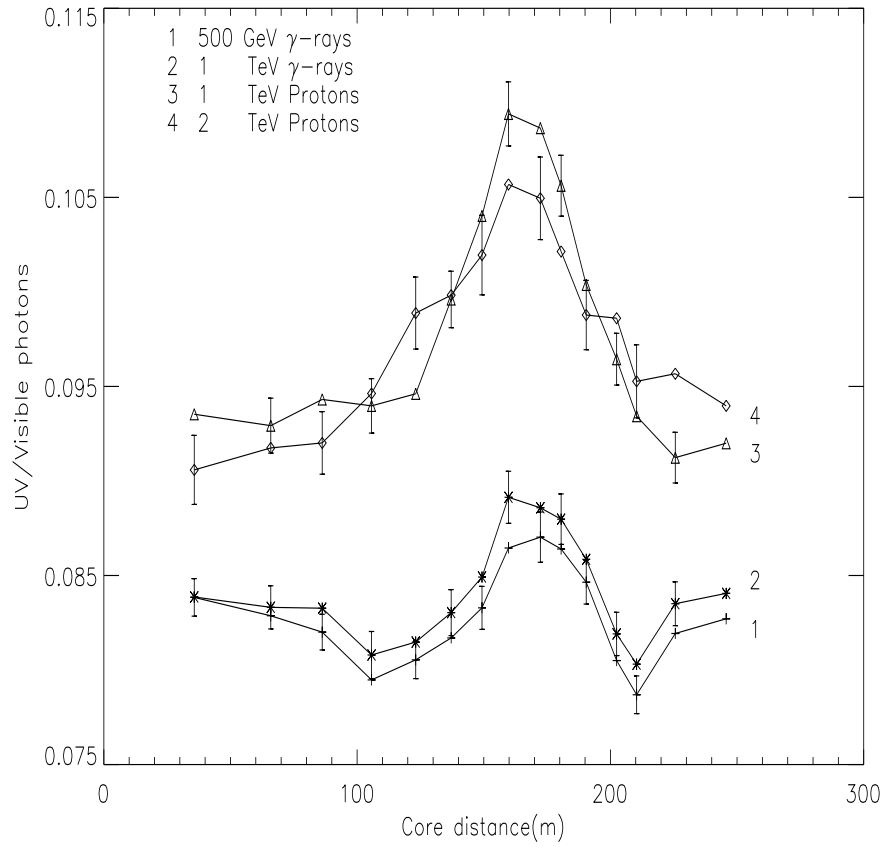


Figure 8: Radial variation of the ratio of UV to visible photons in Čerenkov light generated by protons (1 & 2) and  $\gamma$ -rays (3 & 4) at two primary energies. Alternate error bars are shown for clarity.

study the average shower properties as this is much faster than the detailed simulations. We then apply a detailed wavelength dependent corrections due to the attenuation of Čerenkov photons during their propagation in the atmosphere. This has been done for  $\gamma$ -ray and proton primaries of various energies and for three observation levels. It has been found that the fraction of the transmitted Čerenkov photons at an observation level of 2 *km* above sea level is about 36% more than that at sea level. This is primarily because the average distance to shower maximum is reduced resulting in lesser absorption. Even though the effective collection area is reduced at a higher altitude, the light intensities are larger near the shower core. In addition, increased UV content in the Čerenkov light makes higher observation levels better suited for atmospheric Čerenkov work. Simulations carried out for Mt. Hopkins observatory site (altitude of 2.3 *km*) suggest an advantage factor in the range 1.2-1.4 compared to sea level [29], is consistent with the present result. We also derived the observed Čerenkov photon spectrum for a  $\gamma$ -ray of energy 3 TeV at an observation altitude of 2 *km*. This spectrum agrees well with that reported by Mirzoyan, *et al.*[30] for HEGRA observation level.

The use of a UV filter to preferentially accept Čerenkov light has been suggested even though its efficiency in improving the signal to noise ratio of an atmospheric Čerenkov telescope is in doubt [29]. On the other hand pushing the sensitivity to near UV wavelengths does improve the system sensitivity [23, 27]. Also using suitable filters to suppress the photo-tube sensitivity in the visual band, existing imaging telescopes have been modified so that observations could be made during moderately moonlit nights. This technique has been shown to be successful in detecting *TeV*  $\gamma$ -ray signal from Crab and Mkn 421 despite higher energy threshold and reduced sensitivity [25, 26].

It has been observed by Zyskin, *et al.*, [24] that the relative signal strengths in the UV range (200-300 *nm*) to that in the visible range (300-600 *nm*) increases with the angular size of the image in the visible. It increases up to  $(8 \pm 1.8)\%$  for large images ( $\sqrt{a \cdot b} \sim 0.5^\circ$  where *a* and *b* are the semi-major and semi-minor axis of the image in the optical). This could be due to the fact that those showers whose maximum is closer to the observation level produce larger Čerenkov images. This is equivalent to raising observation level which effectively reduces the attenuation of UV photons as discussed in §4.1 From the present calculations the relative signal strength at a primary proton energy of 4 TeV (energy threshold of Zyskin *et al.*, [24]) is estimated to be  $\sim 10\%$  which is quite consistent with their measurement. It may be noticed that the wavelength ranges used by Zyskin *et al.*, is broader in UV and while the visible band in our estimate was modified to match theirs. However the observed Čerenkov photon spectrum falls steeply below  $\sim 300$  *nm*, as could be seen in figure 6. Extending the wavelength range below 270 *nm* does not change the UV content significantly.

We find that the relative strengths of UV photons to the visible is higher in the case of proton primaries by about 16% at 50 GeV and decreases to 12% at 1 TeV. Hence, the hadron discrimination efficiency based on the UV content in Čerenkov light is relatively better at lower primary energies and at near core distances. Thus, measurement of relative UV content of a shower could be a good parameter in order to discriminate against hadrons especially for large ground based arrays with low energy thresholds ( $\sim 20 - 50$  GeV) and employing the wavefront sampling technique [34, 35, 36, 38, 39]. However one has to keep in mind that for this technique to be successful one has to make a very accurate (better than  $\sim 1\%$ ) estimate of the UV and visible light contents of the shower.

## References

- [1] Hartman, R. C., *et al.*, , 1999, *Astrophys. J. Suppl.*, 123, 79.
- [2] Cronin, J. W., Gibbs, K. G. and Weekes, T. C., 1993, *Ann. Rev. Nucl. Part. Sci.*, 43, 883.
- [3] Fegan, D. J., 1997, *J. Phys. G: Nucl. Particle Phys.*, 23,1013.
- [4] Schubnell, M. S., *et al.*, , 1996, *Astrophys. J.*, 460, 644.
- [5] Ong, R., 1998, *Phys. Rep*, 305, 93.
- [6] Chitnis, V. R. and Bhat, P. N., 2001, *Astropart. Phys.*, 15, 29.
- [7] Knapp, J. and Heck, D., 1998, EAS Simulation with CORSIKA, V5.62: A user's Guide.
- [8] Heck, D. *et al.*, 1998, Forschungszentrum Karlsruhe Report, FZKA 6019.
- [9] Nelson, W. R., 1985, The EGS4 Code System, SLAC Report 265.
- [10] Fesefeldt, H., 1985, Report PITHA-85/02, RWTH Aachen.
- [11] Pyrke, C. L., 2000, Astro-ph Preprint Archive, astro-ph/0003442.
- [12] US Standard Atmosphere, 1962, (US Govt. Printing Office, Washington D. C.).
- [13] Bhat, P. N., 1998, "*High Energy Astronomy & Astrophysics* ' ", Proc. of the Int. Colloquium to Commemorate the Golden Jubilee year of the Tata Institute of Fundamental Research, Ed.: P. C. Agrawal and P. R. Vishwanath, University Press, 370.
- [14] Chitnis, V. R. and Bhat, P. N., 1998, *Astropart. Phys.*, 9, 45

- [15] Ford, R. L. and Nelson, W. R., 1978, SLAC Report #210.
- [16] Lythe, G. D., 1990, *Search for high energy gamma rays from 1987A*, JANZOS Collaboration, Institute for Cosmic Ray Research, University of Tokyo, p362, 368.
- [17] Gaisser, T. K. and Hillas, A. M., 1977, Proc. 14<sup>th</sup> Int. Cosmic Ray Conf., Plovdiv, 8, 353.
- [18] Rao, M. V. S. and Sinha, S., 1988, *J. Phys. G: Nucl. Particle Phys.*, 14, 811.
- [19] Gandhi, V. N., 1992, *Ph D thesis*, University of Bombay (unpublished) p44-47.
- [20] Rao, M. V. S. and Sreekantan, B. V., 1998, *Extensive Air Showers*, Tata McGraw Hill, p23-24.
- [21] Zatsepin, V. I. and Chudakov, A. E., 1962, *Sov Phys.-JETP*, 15, 1126.
- [22] Elterman, L., 1968, US Airforce Cambridge Research Laboratory Report AFCRL-68-0153.
- [23] Goret, P., *et al.*, , 1988, Nucl. Inst. Meth., A270, 550.
- [24] Zyskin, Yu. L., *et al.*, , 1981, Proc. 20<sup>st</sup> Int. Cosmic Ray Conf., Moscow, 2, 342.
- [25] Sarazin, X., *et al.*, 1996, *Astropart. Phys.*, 4, 227.
- [26] Chantell, M. C., *et al.*, 1977, *Astropart. Phys.*, 6, 205.
- [27] Pesci, A., 1993, *Towards a Major Atmospheric Čerenkov Detector - II*, Calgary (Canada), Ed. R.C. Lamb, 192.
- [28] Miller, R. S. and Westerhoff, S., 1998, Astro-ph Preprint Archive, astro-ph/9812153.
- [29] Patterson, J. R. and Hillas, A. M., 1989, Nucl. Inst. Meth., A278, 553.
- [30] Mirzoyan, R., *et al.*, 1994, Nucl. Inst. Meth., A351, 513.
- [31] Chitnis, V. R. and Bhat, P. N., 1999, *Astropart. Phys.*, 12, 45
- [32] Greisen, K., *Prog. in Cosmic Rays Phys.*, 3, 1, 1956.
- [33] Rao, S., *Ph. D. Thesis*, (University of Bombay), Unpublished, 1981.
- [34] Ong, R., 1996, *Il Nuovo Cim.*, 19, 971.

- [35] “Celeste” proposal to the IN2P3 of the CNRS, March 1996, “<http://wwwcenbg.in2p3.fr/Astroparticule>”
- [36] Arqueros, F., *et al.*, 1997, “*Towards a Major Atmospheric Čerenkov Detector - V*”, Berg-en-Dal, Kruger National Park (South Africa), Ed: O. C. de Jager., p 240.
- [37] Hofmann, W., *et al.*, “*Towards a Major Atmospheric Čerenkov Detector - V*”, Berg-en-Dal, Kruger National Park (South Africa), Ed: O. C. de Jager., p 405, 1997.
- [38] Ong, R. and Covault, C. E., 1997, “*Towards a Major Atmospheric Čerenkov Detector - V*”, Berg-en-Dal, Kruger National Park (South Africa), Ed: O. C. de Jager., p 247.
- [39] Tümer, O. T. *et al.*, 1990, Nucl. Phys. B (Proc. Suppl.), 14A, 351.
- [40] Weekes, T. C., *et al.*, “*Towards a Major Atmospheric Čerenkov Detector - V*”, Berg-en-Dal, Kruger National Park (South Africa), Ed: O. C. de Jager., p 433, 1997.